

A High Spatiotemporal Resolution Ultrasonic Ranging Technique With Multiplexing Capability

Zehua Dou¹, Dmitriy Karnaushenko¹, Oliver G. Schmidt¹, and Daniil Karnaushenko¹

Abstract—In this article, a high-performance water-coupled ultrasonic ranging technique is presented. We improved the conventional time-of-flight (ToF) ranging technique based on digital correlation of pseudorandom noise (PRN) waveforms by introducing signal carrier phase shift detection with an I/Q coherent reception method. In this way, the spatial resolution is dominated mainly by the digitization resolution of the analog-to-digital converter (ADC) used in the receiver circuit. Submicrometer resolution is achieved in the entire full-scale-range (FSR) while keeping the ADC sampling rate at the Nyquist sampling limit of the carrier frequency of ranging signal. In this study, we use quadrature amplitude modulation (QAM) waveforms of a set of 1023-bit GPS Gold codes with 8 MHz carrier as a ranging signal. Experiments carried out in a water vessel reveal micrometer-level accuracy and precision for quasi-static and dynamic cases. It is experimentally illustrated that the proposed method is capable of multiplexing. The optimal ranging performance is approached by selecting an appropriate set of systemic technical parameters and ranging signals. This allows to define the figure of merit (FOM) indicating the performance upper bound of such a ranging system.

Index Terms—Correlation, high spatial resolution, phase detection, pseudorandom noise (PRN) waveforms, time of flight (ToF), ultrasonic ranging.

I. INTRODUCTION

HIGH-PERFORMANCE ranging techniques operating in intermediate (10^{-2} – 10^1 m) full-scale range (FSR) are essential for next generation human machine interfaces [1]–[3], Internet of Things (IoT) services [4], navigation of autonomous systems [5], [6], and medical tools [7] to name

Manuscript received July 21, 2021; revised September 10, 2021; accepted October 1, 2021. Date of publication October 14, 2021; date of current version November 3, 2021. This work was supported in part by the German Research Foundation DFG (Gottfried Wilhelm Leibniz Prize granted in 2018) under Grant SCHM 1298/22-1 and Grant KA5051/1-1 and in part by the Leibniz Association (Leibniz Transfer Program T62/2019). The Associate Editor coordinating the review process was Dr. Yixin Ma. (Corresponding authors: Oliver G. Schmidt; Daniil Karnaushenko.)

Zehua Dou, Dmitriy Karnaushenko, and Daniil Karnaushenko are with the Leibniz Institute for Solid State and Materials Research Dresden (Leibniz IFW Dresden), 01069 Dresden, Germany (e-mail: z.dou@ifw-dresden.de; dmitriy.karnaushenko@ifw-dresden.de; d.karnaushenko@ifw-dresden.de).

Oliver G. Schmidt is with the Leibniz Institute for Solid State and Materials Research Dresden (Leibniz IFW Dresden), 01069 Dresden, Germany, also with the Material Systems for Nanoelectronics (Chemnitz University of Technology), 09107 Chemnitz, Germany, also with the Center for Materials Architectures and Integration of Nanomembranes (MAIN) (Chemnitz University of Technology), 09126 Chemnitz, Germany, and also with the Nanophysics, Faculty of Physics (TU Dresden), 01062 Dresden, Germany (e-mail: oliver.schmidt@main.tu-chemnitz.de).

Digital Object Identifier 10.1109/TIM.2021.3120129

a few. Among them there are modern application scenarios such as tracking of microrobots [8], [9] or minimally invasive medical catheters [10] and endoscopes [11], [12]. Ranging systems for these applications need to be capable of providing positions of multiple objects moving at submillimeter velocities with micrometer-level (~ 10 μ m) spatial resolution, accuracy, and precision at high ranging speed, i.e., frame rate over 100 Hz in liquid coupled environment where low signal-to-noise ratio (SNR) is usually addressed [9]. However, conventional systems relying on contact or near-field position sensors [13] operate at too small FSR (10^{-3} – 10^{-2} m) compared with the dimension of the human body and the near inhabited environment. And the FSR of radio frequency (RF) electromagnetic (EM) ranging systems is too large to be able to obtain sufficiently high spatial resolution, accuracy, and precision, mainly due to the high propagating speed of EM waves [14]. Optical sensing technologies, instead, are strongly dependent on optical properties of the environment limiting the FSR (penetration depth) due to scattering, absorption, and reflection [15], [16]. Sophisticated optical ranging systems are usually complex and expensive too [17], [18]. In contrast to EM waves, ultrasonic waves propagate at much slower speed with low attenuation coefficients in air and water. This provides an excellent opportunity to accurately and precisely resolve wave propagation time delay with high resolution within the intermediate distance using relatively simple electronics [19]. Meanwhile, modern piezoelectric materials and MEMS technologies have led to cheap ultrasonic transducers with high energy conversion efficiency, high frequency carriers and bandwidth, as well as small footprint. These transducers have become mass products on the market [20] and are key components for high-performance low-cost ultrasonic ranging.

Nowadays ultrasonic ranging systems commonly rely on digital correlation-based time-of-flight (ToF) techniques that arguably provide optimal SNR levels with simple transducers and electronics. Ranging with these techniques is commonly performed digitally using nowadays data converters and processing units [21]. Briefly about these techniques, a ranging signal is transmitted first, and after propagation time delay, the received passband signal is directly sampled and digitized by an analog-to-digital converter (ADC). A correlation of the received signal and the transmitted signal is performed digitally to resolve ToF that is then transformed to distance with a proper knowledge of sound speed. Previous studies

reveal that the spatial resolution, accuracy, and precision of an ultrasonic ranging system relying on the direct digitization method are proportional to the ADC's sampling rate [22]–[25], and the reason is twofold. On the one hand, a digital system is only capable of resolving time intervals equivalent to the sampling period [22]. On the other hand, the ToF estimation error caused by digitization error of the received passband signal due to asynchronous sampling spectrum leakage can be improved by increasing the ADC sampling rate [25], [26]. Therefore, to obtain ranging results with high spatial resolution, accuracy, and precision performing a direct digitization method, ADC sampling rates of about ten times higher than a carrier frequency are necessary, especially in low SNR circumstances [23], [24], [26]–[28]. Such direct digitization correlation-based ToF ranging systems are usually employed in air coupled applications operating at low frequency, e.g., 20–40 kHz ultrasonic waves. Usually, regular electronics is used for these applications, which is able to process datapoints of acquired signals at rates of 100 kHz–1 MHz in real time [29]–[33]. Generally, these systems are capable of ranging with millimeter-level spatial resolution and accuracy [29]–[33].

However, in order to realize micrometer-level spatial resolution, accuracy, and precision using a direct digital correlation approach in water-coupled environments with the sound speed of about four times higher than in air, one needs to sample the received signal at higher rates, and then digitally process the acquired massive set of datapoints with high-performance field programmable gate arrays (FPGAs) or digital signal processing (DSP) circuits. For instance, one would need to sample the passband signal with 1 GHz or even higher rate for an extended period of time to reach 1 μm resolution within the intermediate FSR for ultrasound propagating in water, where the speed of sound in water is assumed to be approximately 1500 m/s at room temperature. Long acquisition period with a high sampling rate not only increases system costs but also create additional signal processing complexity that potentially decreases the ranging speed, i.e., the temporal resolution [34].

Besides the correlation ToF ranging scheme, high spatial resolution is achievable with phase shift detection of mono-frequency ultrasonic waves. This approach is capable of resolving subwavelength distances between a transmitter and receiver at relatively low sampling rates [35]. For an ideal case, phase of a mono-frequency signal can be accurately recovered by sampling the signal at its Nyquist limit, i.e., twice the signal's fundamental frequency. To further eliminate the periodical ambiguity and obtain knowledge of the distance in a desired FSR, combinations of the carrier phase shift detection with correlation-based ToF estimation were proposed and implemented [35], [36]. Briefly, such combinations utilize multifrequency ranging signals where subwavelength range is refined by phase shift detection at only the carrier frequency, and a correlation ToF ranging result obtained at low sampling rates is then used to determine the integer number of wavelengths within the FSR [35], [36]. In such a way, the sampling rate (F_s) to carrier frequency (F_c) ratio (F_s/F_c) can be held at a relevantly low value. Unfortunately, when affected

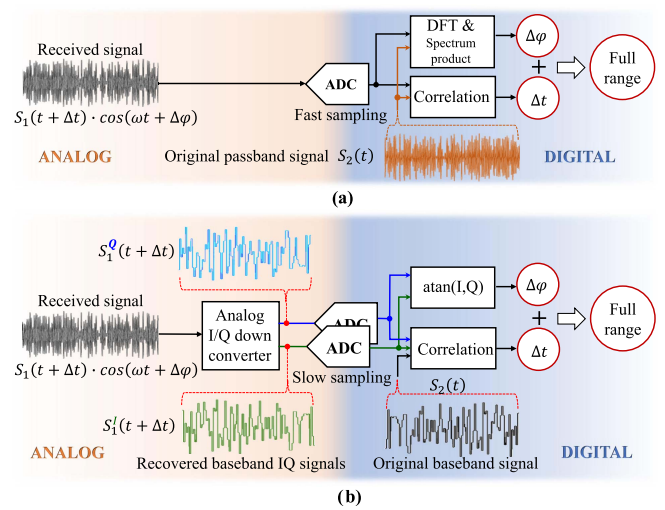


Fig. 1. Schematic comparison between the conventional approach and the improved method. (a) Schematic of the direct passband digitization approach where high F_s/F_c is required. (b) Schematic of the improved ranging method with zero-IF baseband and direct carrier phase shift detection at an effective F_s/F_c value of 2.

by noise, the ToF estimation carried out at low sampling rates unavoidably leads to ranging error corresponding to multiple sampling intervals due to asynchronous sampling spectrum leakage digitization error. Therefore, with regard to high-performance ranging with low ADC F_s/F_c value, baseband signal processing is more attractive, since the baseband signal contains all the necessary information required by the correlation ToF ranging scheme, and meanwhile it varies much slower in time due to the high-frequency carrier components being eliminated. This means that performing correlation ToF ranging on a baseband signal with the same F_s/F_c value is more accurate and precise than on its passband signal.

Therefore, the basic idea of our method is to perform a combination of correlation ToF ranging and carrier phase detection using baseband signal recovered from passband signal by applying an analog synchronous down conversion at the carrier frequency. In this way, the correlation ToF ranging technique can be performed on the recovered baseband signal sampled at the carrier frequency to accurately and precisely obtain a distance of multiple wavelengths. Meanwhile, the carrier phase can be recovered from the in-phase and quadrature channels of the down converter to obtain a subwavelength range refinement [37]. In this article, the proposed combination of correlation ToF and carrier shift detection with low F_s/F_c value is realized by introducing an analog quadrature I/Q (in phase/quadrature) down-conversion scheme. That scheme allows for a zero-intermediate frequency (IF) baseband signal operation and a direct carrier phase shift detection. In this way, the spatial resolution is mainly determined by the ADC digitization resolution, and an effective F_s/F_c value of 2, i.e., one sample per carrier period on both I and Q channels, highly reduces the cost of systemic infrastructure that could be caused by a signal processing complexity using conventional direct digitization approach of passband signals. The two different ranging schemes are illustrated in Fig. 1.

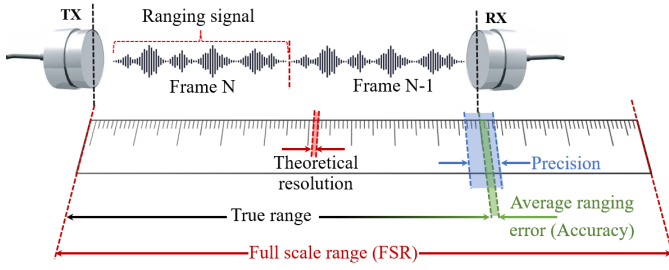


Fig. 2. Dual-transducer through transmission configuration. The accuracy and precision are defined as the average value and the standard deviation of ranging error, respectively.

Furthermore, we analyze and provide relations between technical parameters of the hardware and ranging signals deriving the overall systemic performance. We verified the performance with a dual-transducer-through-water ultrasound transmission system (Fig. 2) in a vessel with a maximum FSR of 200 mm. We used QAM waveforms of 1023-bits Gold codes with 8 MHz carrier signal ($\lambda = 187.5 \mu\text{m}$). The passband ultrasound signal was down converted to a baseband signal with a radio receiver and sampled at 8 MHz sampling rate applying two 10-bit ADCs in an I/Q scheme. This allowed us to reach a submicrometer-level spatial resolution of 45.7 nm [$187.5 \mu\text{m}/(4 \times 1024)$], an accuracy of 2.31 μm , and a precision of 0.82 μm .

Following the introduction, this article is divided into four sections. Section II theoretically illustrates the proposed improvement of correlation-based ToF ranging with carrier phase shift detection and the modulation scheme of binary pseudorandom noise (PRN) sequences to obtain appropriate ranging signals. Section III experimentally investigates the performance of the improved ranging method using two piezoelectric transducers as emitter and receiver. The results of these measurements are analyzed, and the relations between systemic technical parameters and ranging performance metrics are discussed as well. Finally, the conclusion and outlook are given in Section IV.

II. RANGING METHOD

A. Working Principle of the Improved Ranging Scheme Introducing an Analog I/Q Down Converter

In this work, all discussions are based on the through-transmission configuration (Fig. 2). The working principle of the correlation-based ToF ranging technique is briefly described for such a configuration. The ranging signal is continuously transmitted and received between an object and an ultrasonic transducer. Due to the propagation time delay, the received signal possesses a time offset compared with the originally transmitted signal, which is illustrated in Fig. 3(a), where a mono-frequency harmonic signal is used only for a clear perception (the real signal is described in Sections II-B and II-C). In order to get rid of the massive data processing burden caused by the high ADC sampling rate, required when using the conventional digitization and correlation approach [Fig. 1(a)], an analog I/Q down converter is used allowing to remove carrier frequency from the signal.

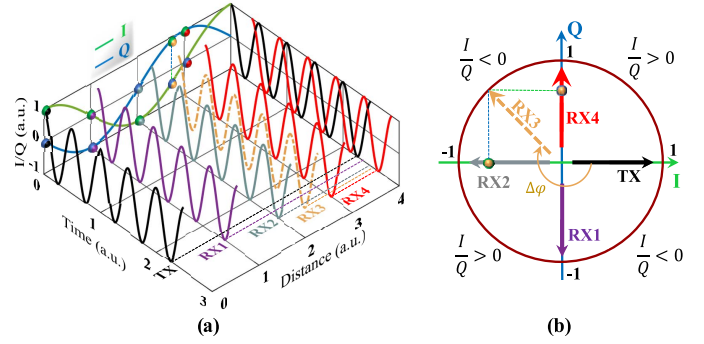


Fig. 3. Working principle of the ToF ranging and carrier phase shift detection using the scheme with an analog I/Q down converter. (a) Phase shift and time offset between of a transmitted and received mono-frequency signals due to wave propagation. The down converted I/Q data of each received signal is represented by dots at any single sampled point in time. (b) Four-quadrant inverse tangent function eliminating phase detection ambiguity in $[-\pi, \pi]$, where the phase angles of the four received signals are indicated by arrows with corresponding colors.

These two I and Q signals are then used for a direct carrier phase detection and correlation [Fig. 1(b)]. In this way, it is possible to resolve distance below one wavelength while keeping an equivalent F_s/F_c value of 2 [Fig. 1(b)]. More precisely, the received passband signal is firstly down converted to zero-IF, and then the baseband signal is digitized by the ADC at a sampling rate same as the carrier frequency for both I and Q channels. The carrier phase shift is then calculated from values of the I and Q channels by using the four-quadrant inverse tangent function [Fig. 3(b)] effectively resolving the ambiguity in $[-\pi, \pi]$ at each sampling point. In this scheme, the spatial resolution is directly dependent on the ADC digitization resolution. Due to the nonlinearity of the inverse tangent function, the spatial resolution from phase shift of a mono-frequency signal is only evaluated as an average value that is written in (1) where λ is the wavelength of ultrasound, and N_{ADC} is the ADC resolution in bit [36], [37]

$$r_{\text{fine}} = \frac{v}{4 \cdot 2^{N_{\text{ADC}}} \cdot f_c} = \frac{\lambda}{4 \cdot 2^{N_{\text{ADC}}}}. \quad (1)$$

Formula (1) indicates that the phase shift detection technique can easily achieve submicrometer-level spatial resolution using RF ultrasound ($\sim\text{MHz}$) and a regular 10-bit ADC. Therefore, we term the spatial resolution obtained from carrier phase shift as the “fine resolution.” For instance, a fine resolution of 45.7 nm (mean value) can be theoretically achieved using a carrier frequency of 8 MHz, where the sound speed in water is assumed to be 1500 m/s at room temperature, i.e., the wavelength is $\lambda = 187.5 \mu\text{m}$.

In order to further resolve a range of multiple wavelengths to obtain a full knowledge of the distance within a desired FSR, a digital correlation of complex numbers assembled from I and Q channels of digitized baseband signal and the originally transmitted one is performed. More specifically, the integral of the product of the two signals is calculated at all offsets with intervals corresponding to the ADC sampling rate. When the received signal and the transmitted signal perfectly overlap, the maximum correlation value peak is obtained.

Afterward, the total offset between the reference signal and the received signal is converted into the wave propagation time delay. In other words, the ToF is counted as a number of ADC sample clocks when using the digital correlation approach. In this way, the distance between an object and an ultrasonic transducer can be obtained with the knowledge of the wave propagating speed in the medium. Therefore, the spatial resolution of correlation ToF is given in (2) [21], where v is the sound speed in the medium, and F_s is the ADC sampling rate. In our approach, the spatial resolution from ToF ranging technique is equal to the carrier wavelength and, therefore, it is termed the “coarse resolution”

$$r_{\text{coarse}} = \frac{v}{F_s}. \quad (2)$$

In short, the improved combination of the carrier phase shift detection and correlation-based ToF ranging technique with an analog I/Q down converter allows for submicrometer resolution in ranging systems without any ambiguities in the entire FSR using simplified electronics while keeping an equivalent ADC sampling rate of received baseband signal as the Nyquist sampling limit of carrier frequency. Meanwhile, such a sampling rate should be capable of accurately and precisely digitizing the baseband signal and providing reliable ToF ranging results even in noisy environments.

In addition, to eliminate any ambiguities and improve FSR, accuracy, resolution, and precision, the ranging signal must be suitable for the I/Q down-conversion carrier phase detection scheme, and it should possess excellent correlation property with a clearly distinguishable autocorrelation peak within a longer period. Ranging signals with such properties are available using binary PRN codes and various digital modulation schemes.

B. Pseudorandom Codes: Gold Codes

Binary PRN sequences are a set of special ascertained vectors with outstanding autocorrelation and cross correlation properties, i.e., orthogonality, such as Barker codes [38], Zadoff–Chu sequences [39], Gold codes [29], Kasami codes [30], maximum length sequences [40], and Golay codes [41] to name a few. The excellent autocorrelation properties of these sequences provide an opportunity to accurately and precisely distinguish the positions of correlation peaks. In addition, the low cross correlation among different codes reduces interference when simultaneously tracking numerous objects with individual PRN identifications. Among commonly used PRN sequences of defined length, Gold codes provide a large set of orthogonal sequences allowing for a large number of objects to be tracked at the same time. In this article, 1023-bit Gold codes are used for demonstration purposes, and they are generated according to the official global positioning system (GPS) interface control document [42]. This set of Gold codes contains 32 different sequences, and their highest periodical autocorrelation and cross correlation values are 1023 and 65, respectively (Fig. 4). The ratio of 15.07 of the two values is defined as the dynamic range of the set of PRN codes.

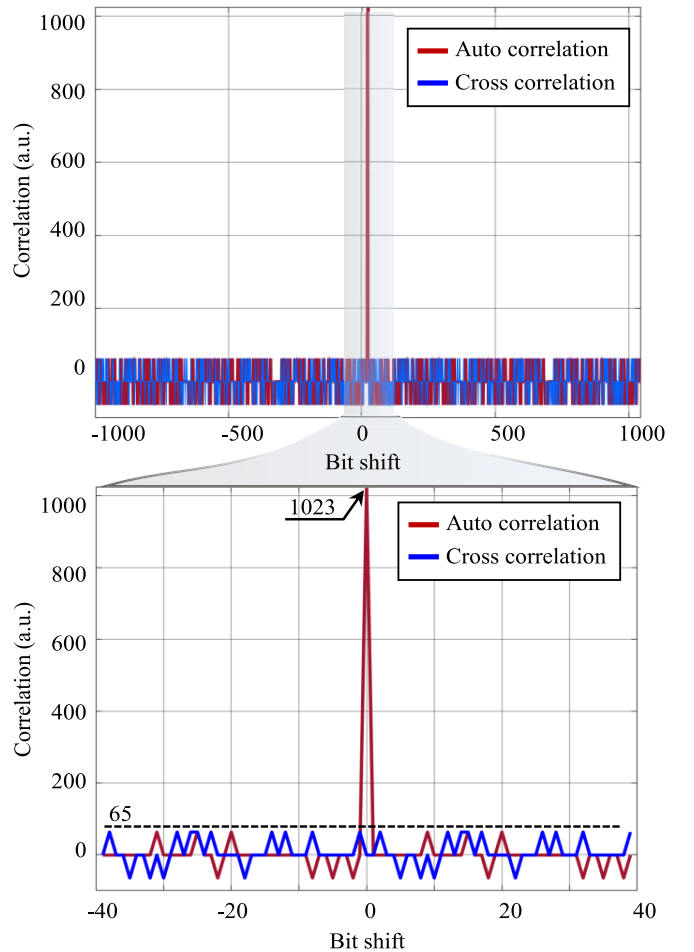


Fig. 4. Periodical autocorrelation and cross correlation of 1023-bit GPS Gold codes.

C. From Gold Codes to Ranging Signals

For an efficient transmission of Gold codes with a piezoelectric transducer, the signal should be generated at a specific frequency achieved by a certain modulation scheme, such as amplitude shift keying (ASK) [43], frequency shift key (FSK) [36], binary phase shift keying (BPSK) [44], quadrature phase shift keying (QPSK) [45], and quadrature amplitude modulation (QAM) [46]. The bandwidth of a passband signal modulated with a single carrier frequency is directly related to the PRN code symbol rate as $BW = 2 \cdot f_{\text{sym}}$ [44], where f_{sym} is the symbol rate, which must fit the bandwidth of the transducer. For a specified code length and the limited bandwidth of the acoustic system, the ranging frame rate at CW working mode, as a significant performance metric, is defined as the reciprocal of the ranging signal’s period τ , as written in (3), where BW is the bandwidth and N_{sym} is the total amount of symbols

$$\text{FPS} = \frac{1}{\tau} = \frac{BW}{2 \cdot N_{\text{sym}}}. \quad (3)$$

For 1023-bit Gold code sequences, an odd length, only a few modulation schemes are realistically available, namely binary modulation techniques including BASK and BPSK

with 1023 symbols, 8-QAM and 8-PSK with 341 symbols, as well as 2048-QAM with 93 symbols. Other higher order modulation schemes are not physically feasible being limited by the digitization resolution of digital-to-analog converter (DAC) used in the transceiver circuit. According to (3), the ranging frame rates are 23 and 586 Hz when using ranging signals based on binary modulation and 8-QAM (or 8-PSK) schemes, respectively. In order to maintain a high ranging speed over 1000 Hz, high-order 2048-QAM scheme is necessary allowing to reduce the total amount of symbols to be transmitted. In this scheme, each 1023-bit Gold code sequence is disassembled into 93 symbols. Each 11 bits symbol encodes amplitude and phase as shown in the I/Q constellation diagram [Fig. 5(a)]. The ranging signal of a Gold code sequence after modulation is plotted in Fig. 5(b) as an example. Furthermore, the bandwidths of QAM waveforms are two times the symbol rate as indicated in Fig. 5(c). Practically, when using such a modulation scheme, a frame rate of 2.15 kHz can be reached with a bandwidth of 400 kHz, which is sufficient for, e.g., tracking of autonomous robotic systems. Moreover, using these parameters, the FSR is 697 mm calculated as (4), in which v is the sound speed in the medium. The resulted FSR is in the desired intermediate range

$$\text{FSR} = \frac{v}{\text{FPS}} = \frac{2 \cdot v \cdot N_{\text{sym}}}{\text{BW}}. \quad (4)$$

In summary, the signal processing flow of our proposed ranging scheme is demonstrated in Fig. 6, where we use 2048-QAM Gold code sequences as ranging signal. Briefly, the ranging signal is transmitted and received in a continuous mode [Fig. 6(a)]. Each frame of received ranging signal is down converted to zero-IF baseband signal, and then sampled and digitized at the carrier frequency. The integer number of wavelengths is obtained from ToF ranging technique using the recovered baseband signal [Fig. 6(b) and (c)], while the subwavelength range is then calculated from I and Q data at each sampling point [Fig. 6(a)]. Finally, the ranging values are obtained by combining the correlation ToF technique and the carrier phase shift performed on the digitized baseband signal. This results in high spatiotemporal resolution, accuracy, and precision.

III. EXPERIMENTAL RESULTS AND DISCUSSIONS ON THE PROPOSED RANGING SCHEME

A. Experimental Setup

The schematic representation of the experimental ranging setup is shown in Fig. 7. The mechanical part includes a holder platform, a programmable motorized stage with a 200 mm FSR and 15 nm step resolution (X-LSM200A-E03, Zaber Technologies Inc.), and a vessel. Two piezoelectric disks [model 53020, PI Ceramic GmbH Fig. 7(b)] with 8 MHz resonance frequency and 2 MHz bandwidth are used as ultrasonic transducers for both the object and receiver. They are aligned and placed under water in the vessel. One ultrasonic transducer is fixed at a certain position on the holder platform and another one is attached to the motorized stage controlling the distance between these two transducers

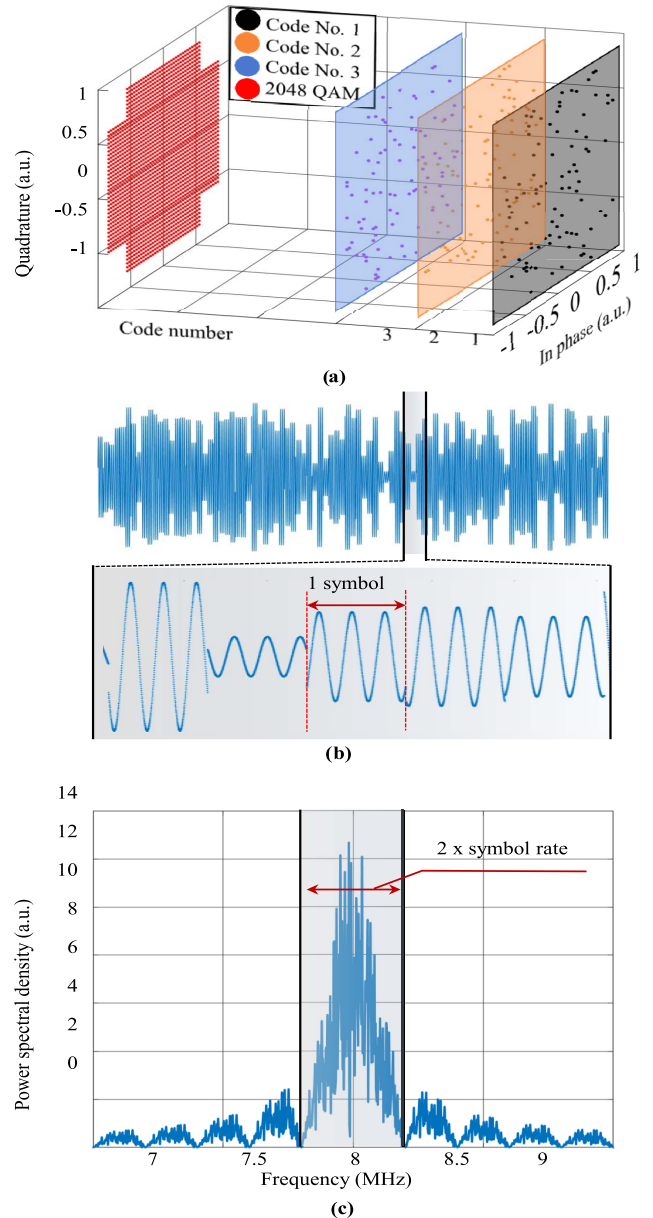


Fig. 5. 2048-QAM of 1023 bits Gold codes. (a) Constellation diagram where each sequence addresses only 93 symbols. (b) Modulated signal, in which the carrier frequency, phase, and amplitude abrupts can be observed. (c) Power spectrum of modulated ranging signal where the sidelobe energy is -15 dB of the main-lobe energy.

[Fig. 7(a)]. A Keysight 33626A arbitrary function generator is used to excite the emitter producing ultrasonic ranging signals. The receiver transducer is connected to the software defined radio (SDR) receiver (rsp2pro, SDRplay Ltd.) relying on I/Q coherent down conversion and reception with 2×10 -bit ADCs digitizing the baseband signals. The digital signal is transferred to a PC, where the ToF ranging technique and phase shift detection are realized by MATLAB programs with results displayed in real time. The local oscillation frequency of the SDR I and Q channels is locked to the carrier frequency using a phase locked loop (PLL) to omit ranging errors occurring due to a slight frequency mismatch between local oscillators of transmitter and receiver.

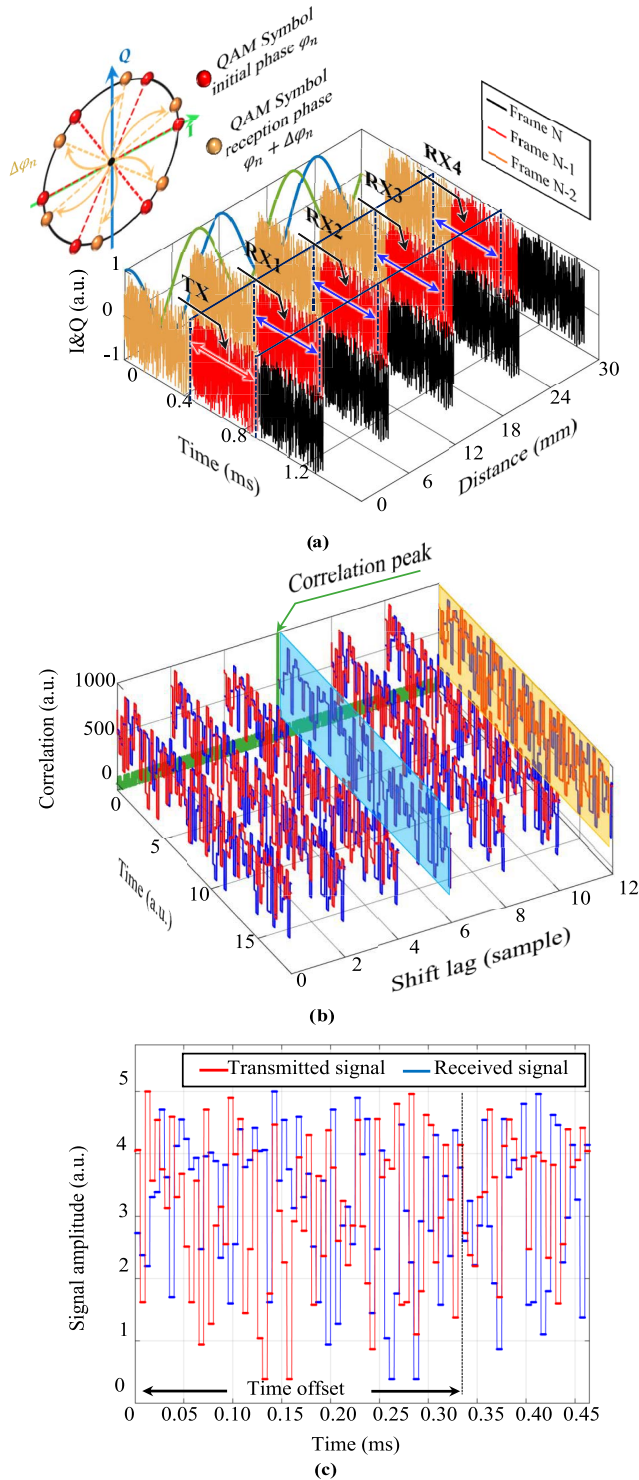


Fig. 6. Combined ranging scheme. (a) Combined ranging scheme including carrier phase shift detection and correlation, where the phase shifts of symbols with different initial phases and phases at reception are illustrated on a unit circle in I/Q complex plane. (b) Schematic representation of correlation-based ToF ranging technique with baseband signals. (c) Condition of the recovered baseband signal with offset to the originally transmitted one (yellow surface in b).

B. Ranging Performance

The distance between the two ultrasonic transducers was precisely controlled by a motorized stage defining a reference

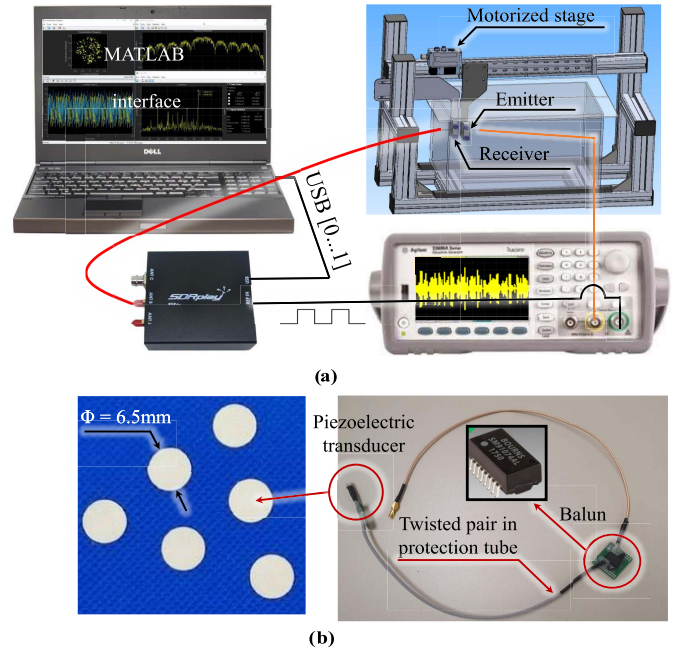


Fig. 7. Schematics of experimental setup to prove the proposed ultrasonic ranging scheme. (a) Schematic sketch of the setup. (b) Piezoelectric transducers used in experiments.

range value. The relative displacement between two transducers, computed by the MATLAB program, was then compared with this reference value. In our experiments, the ranging signal was chosen as discussed in Section II, with the 2048-QAM waveform of a 1023-bit Gold code with 400 kHz bandwidth carried by an 8 MHz ultrasonic wave, i.e., the QAM symbol rate was 200 kHz. The signal was continuously transmitted and received between two transducers without time interval at a frame rate of 2.15 kHz as illustrated in Fig. 6. The measurements were carried out at room temperature, where the sound speed in water is assumed to be 1500 m/s and, therefore, the FSR using above parameters is 697.7 mm. At the receiver side, the ADC sampling rates of both I and Q channels were set to be 8 MHz and the ADC resolution is 10-bit defined by the SDR. These settings correspond to an average value of the spatial resolution of 45.7 nm.

1) *Spatiotemporal Resolution*: First, the aforementioned fine spatial resolution is studied. For this purpose, a relative displacement between two ultrasonic transducers was set to be 1, 2, and 10 μm , respectively, to verify the theoretical spatial resolution. The measured relative displacement in real time is plotted in Fig. 8 indicating the control values as well. The theoretical 45.7 nm average spatial resolution is not reached due to ranging errors caused by external noise. We determine the best feasible spatial resolution by evaluating the smallest distinguishable displacement from the noise floor. The value is derived from the standard deviation of the static state ranging error [28], [35], as written in (5) where d_i and \bar{d} are the real time and mean value of measured displacement values at static states, and n is total amount of frames acquired. Formula (5) is too known as the precision of ranging. Specifically, the precision and the fine spatial resolution share the

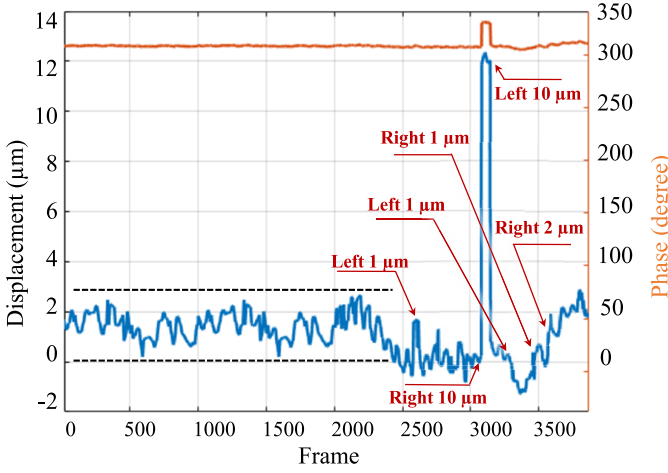


Fig. 8. Real-time ranging results at quasi-static states indicating the micrometer level of fine resolution by means of carrier phase shift detection method.

same meaning in noisy environments where the fine resolution is corrupted by noise

$$\sigma = \sqrt{\frac{\sum (d_i - \bar{d})^2}{n}}. \quad (5)$$

Static state ranging results over the first 2500 frames are shown in Fig. 8, indicating that the standard deviation of the ranging error is less than $2 \mu\text{m}$, which means any displacement larger than $2 \mu\text{m}$ can be clearly resolved.

2) *FSR of the System*: The ability of the ToF ranging technique to eliminate any ranging ambiguity within the FSR is experimentally validated. The initial distance between two transducers was set to be 200 mm, and the relative displacement was set to be greater than one wavelength. The emitter-transducer was fixed on the holder platform and the receiver was attached to the motorized stage. The receiver was moved by the motorized stage from its initial position toward the transmitter (left) and away from it (right) 100 mm with 10 mm/s velocity. It is worth to note that the approximate sound speed of 1500 m/s in the previous measurements is, however, a bit different from the real value, and the deviation leads to small offsets in ranging results, especially when the distance between the two transducers is enlarged. Thus, the sound speed is precalibrated in this measurement.

The real-time ranging results of the proposed ranging scheme are plotted in Fig. 9. It clearly indicates that the periodical ambiguity of the carrier phase detection can be compensated by the correlation ToF ranging technique when the displacement is greater than one wavelength, and the combination of these two ranging approaches allows to achieve the intermediate FSR while keeping high spatial resolution between an object and a receiver. The ranging result also verifies that the proposed ranging scheme is capable of accurately tracking moving objects at a reasonable velocity. Specifically, the 10 mm/s relative velocity of emitter and receiver leads to 53.34 Hz Doppler when using 8 MHz carrier frequency, which is calculated in (6) [47]. In this case, a 53.34 Hz harmonic component remains in the down converted baseband signal.

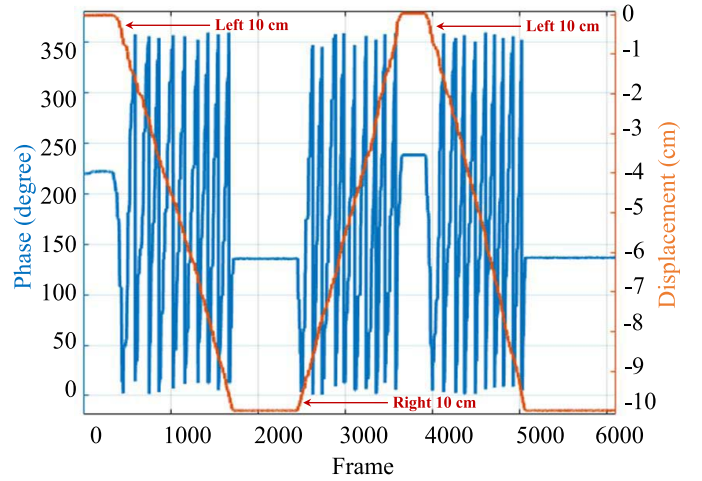


Fig. 9. Real-time ranging results indicating the FSR and the ability of tracking dynamic moving objects.

TABLE I
RANGING ACCURACIES AND PRECISIONS OF A SINGLE OBJECT
AT DIFFERENT SNR LEVELS

SNR (dB)	Accuracy ρ (μm)	Precision σ (μm)
-8	38.99	87.47
-3	37.04	84.39
11	2.31	0.82

However, comparing with the 2.15 kHz ranging frame rate and 8 MHz carrier frequency, the 53.34 Hz Doppler shift has ignorable influence on both correlation and carrier phase shift detection

$$\Delta f = f_c - \frac{f_c}{(1 - \frac{v}{c})} = 8 \times 10^6 - \frac{8 \times 10^6}{(1 - \frac{0.01}{1500})} = 53.34 \text{ Hz}. \quad (6)$$

3) *Accuracy and Precision*: In our laboratory environment, the ranging results are affected by various kinds of noise that are experimentally acquired. The noise resembles that of additive white Gaussian noise (AWGN) with a Gaussian normal distribution of the amplitude and a constant power spectral density as depicted in Fig. 10. For high accuracy and precision, the SNR must be enhanced by, for instance, increasing the amplitude of the ranging signal. The relation between the ranging accuracy, precision, and SNR in the laboratory environment was further experimentally studied under static conditions. The distance between the two transducers was fixed at 200 mm, and the SNR was tuned by the electrical excitation amplitude of the piezoelectric transducer to -8, -3, and 11 dB. The mean value and the standard deviation of the measured relative displacements over time represent the ranging accuracy and precision. The ranging accuracies and precisions over 10 000 frames are summarized for three electrical excitation amplitudes shown in Table I, indicating that the ranging accuracy and precision are significantly improved with increasing electrical excitation. Affected by the AWGN, the position of a correlation peak at lower SNR

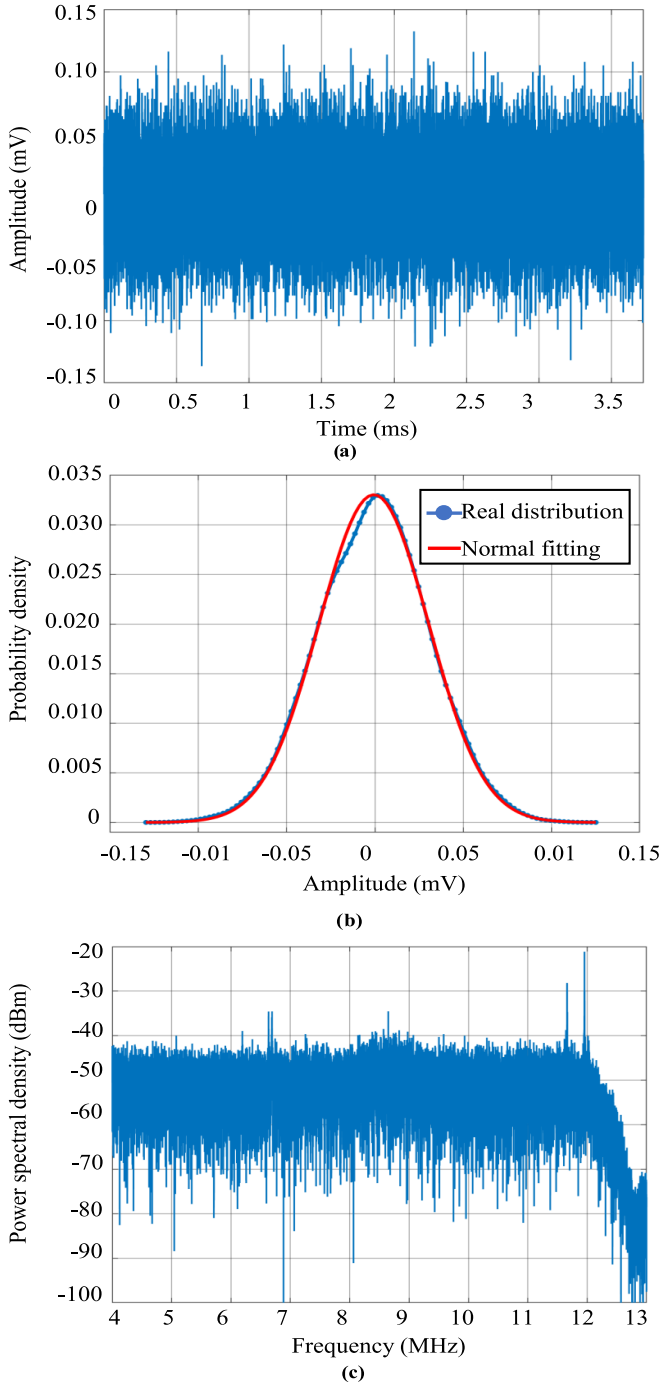


Fig. 10. AWGN collected from the passband of receiver circuit. (a) Noise in time scale. (b) Probability density function of noise amplitude shows a good agreement with Gaussian normal distribution. (c) Power spectral density of the background signal.

levels (-8 and -3 dB) was shifted by one or several sampling clock position(s) in some ranging frames, which leads to poor ranging accuracies and precisions. With an elevated but realistic SNR level of 11 dB, the correlation peak position was correctly determined and the ranging accuracy and precision were $2.31 \pm 0.82 \mu\text{m}$. In other words, the accuracy and precision depend on the correlation peak width and height (i.e., sharpness) as well as the noise level. Since the cross

correlation of the originally transmitted (reference) and the recovered baseband signals is performed, the correlation peak width is the reciprocal of the symbol rate f_{sym} in time scale. Further discussions are simplified by normalizing the amplitude of reference signal. Thus, the peak height is known as the amplitude period product of the received signal, and the peak sharpness, i.e., height to width ratio is written as (7), in which A is the averaged amplitude of received signal, and τ is the period of ranging signal [48]. The amplitude of noise level, i.e., the correlation of AWGN and unit amplitude baseband signal leading to ranging errors is given in (8), where $2 \cdot N_0$ is the double side power spectral density of AWGN [48]. According to the relation of symbol rate, ranging frame rate and PRN code length given in (3), the accuracy (ρ) and precision (σ) are derived in (9) following $\text{SNR} = A^2/N_0 \cdot \text{BW}$, where BW is the bandwidth.

$$k = A \cdot \tau \cdot f_{\text{sym}} \quad (7)$$

$$n = \sqrt{2 \cdot N_0 \cdot \tau} \quad (8)$$

$$\frac{1}{\rho}, \frac{1}{\sigma} \propto \frac{k}{n} = \sqrt{\text{SNR}} \cdot N_{\text{sym}}^{\frac{3}{2}} \cdot \text{FPS}. \quad (9)$$

4) *Multiple Objects Capacity*: The proposed ranging scheme is capable of tracking multiple objects simultaneously by assigning each object an individual modulated PRN waveform as ranging signal. We added up modulated waveforms of Gold codes with numbers 1 to 6 defined in the GPS standard with an offset of two symbols to each other. The combined waveform was transmitted through a piezoelectric transducer effectively mimicking the tracking condition of six objects with different distances to a receiver. In this experiment, the SNR level for each individual code was set to be -8, -3, and 11 dB. The distance between the emitter and receiver was set to be 200 mm using DI water as medium. The mean values of ranging accuracies and precisions of a particular object (code) over 10000 frames are summarized in Table II. We observe that the accuracy of tracking six objects is worse than tracking a single object but the precisions of these two cases are comparable. The accuracy is degraded by interferences caused by the nonideal orthogonality of the PRN codes. Moreover, the multiplexing capacity of modulating Gold codes with 2048-QAM is reduced because the Gold codes lose their original cross correlation properties after modulation. In fact, the dynamic range of the modulated codes decreased from 15.07 to 6.05. In order to increase the multiplexing capacity without degrading the ranging accuracy and precision, PRN codes with ideal orthogonality should be explored in the future [49].

C. Discussions

1) *Ranging Performance of the Experiments*: First of all, the highest frame rate in the above experiments is 2.15 kHz applying QAM ranging signals with 400 kHz bandwidth. Moreover, the experiments verified that the full range between an object and an ultrasound receiver with submicrometer resolution is available by combining both the ultrasound propagation phase shift detection and the correlation-based TOF ranging technique. However, affected by AWGN, the theoretical fine spatial resolution from the carrier phase shift detection is not

TABLE II
RANGING ACCURACIES AND PRECISIONS OF SIX OBJECTS
AT DIFFERENT SNR LEVELS

SNR	11 dB	-3 dB	-8 dB
No. 1	10.38 ± 4.21	157.87 ± 84.01	248.25 ± 109.09
No. 2	22.13 ± 10.78	90.58 ± 31.87	164.06 ± 80.14
No. 3	38.77 ± 18.35	120.70 ± 97.69	287.25 ± 210.32
No. 4	32.19 ± 12.13	81.47 ± 59.49	183.55 ± 70.87
No. 5	21.38 ± 18.06	92.06 ± 63.24	147.28 ± 103.69
No. 6	36.94 ± 2.65	190.75 ± 59.49	291.18 ± 136.89

TABLE III
PERFORMANCE COMPARISON

Techniques	Signals	F_s/F_c	Precision
Direct correlation [52]	Mono-frequency pulse	32	cm level in water @ 500 mm
Direct correlation [30]	31 bits Gold codes DQPSK	26	cm level in air @ 3 dB
Direct correlation interpolated [51]	Mono-frequency pulse	1000	5.64 μ m in water @ 300 mm
This work	1023 bits Gold codes 2048-QAM	2	0.82 μ m in water @ 200 mm

obtained experimentally, and the standard deviation of the ranging error, i.e., the precision is used to evaluate the minimal resolvable displacement of an object. Ranging accuracy and precision are verified to be proportional to the SNR according to statistics of ranging results at three different excitation levels over 10000 frames at three different SNR levels. These experiments reveal that submicrometer precision can be reached using an acceptable electrical excitation voltage of the piezoelectric transducer that does not cause power consumption or safety issues in real applications [50]. We experimentally validated that it is possible to track six signals (objects) simultaneously within a 200 mm FSR using PRN waveforms with reduced orthogonality but with acceptable accuracy and precision.

Table III compares ranging performances of this work and conventional direct acquisition and correlation approaches. The comparison reveals that the sampling rate to carrier frequency ratio (F_s/F_c) is a key factor affecting the precision in conventional direct digital correlation approaches with a direct proportion relation. Specifically, as reported by Jia *et al.* [51], a 1 GHz ADC was used to sample 1 MHz passband ultrasonic signals to realize micrometer-level precision, which unavoidably requires high-speed processing units and memory devices in order to realize real-time ranging system. In contrast, taking the advantage of zero-IF baseband signal processing and direct carrier phase shift detection using analog I/Q down convertor, our method reduces the equivalent F_s/F_c value 500 times realizing a comparable precision level.

2) *FOM of Correlation-Based Ranging Systems*: In reality, the modulation scheme and parameters of ranging signals as well as the physical capabilities of systemic infrastructure, such as the sampling rate and digitization resolution, are all

factors affecting the ranging performance, as indicated by Table III. Therefore, the figure of merit (FOM) is defined to indicate the upper bound of a correlation-based ranging system performance. The FOM is defined as the ratio of ranging speed, i.e., frame rate and precision, which is written as

$$\text{FOM} = \frac{\text{FPS}}{\sigma} \propto \sqrt{\text{SNR}} \cdot \frac{\text{BW}^2}{\sqrt{N_{\text{sym}}}}. \quad (10)$$

In order to position several objects (fixed N_{sym}) with high accuracy and precision (smaller σ value) at high speed, the highest FOM values are desired, which can be achieved by increasing the SNR and bandwidth of the wireless channel. However, the bandwidth of RF ultrasonic channels is physically limited, and the SNR value cannot be infinitely increased in a real application due to various reasons, such as the dynamic range of transducers and safety considerations to name a few. Therefore, once the available SNR and bandwidth of a particular ranging system are determined, the performance upper bound, i.e., the highest FOM value of the system is then fixed. The maximum FOM value stands for the highest ranging speed, accuracy, and precision that can be simultaneously realized by such a system with a specific set of PRN ranging signals whose orthogonality ensures a certain multiplexing capacity. For instance, the FOM of a particular ranging system with maximum SNR of 11 dB and 400 kHz bandwidth is plotted in Fig. 11 in log scale. Specifically, vertical surfaces indicate relation among accuracy, precision, multiplexing capacity, and ranging frame rate for the corresponding SNR value as given by (9). The other surfaces illustrate the relation among ranging frame rate, multiplexing capacity, and given bandwidth values which are written in (3). Moreover, intersection lines between these surfaces provide exact performance metrics values obtained by the specific system working with corresponding SNR and bandwidth values. Thus, the green line in Fig. 11 indicates performance upper bound of a specific system, i.e., the highest precision and ranging frame rate simultaneously achieved for corresponding PRN signals. This is illustrated by the performance metrics of the red, gold, and purple dots realized for different bandwidths and SNR values in Fig. 11. Nevertheless, the multiplexing capacity is determined by the orthogonality of PRN codes, and the FSR can be obtained with a proper knowledge of sound speed as illustrated by (4). The performance upper bound also means that the region out of the highest bandwidth and SNR surfaces is not physically feasible with the system, and the feasible region of our specific system is marked with hash line in Fig. 11.

Nevertheless, the FOM intuitively instructs design of a ranging system to exert its full capability toward real applications. Specifically, for applications desiring longer FSR values, it is always preferred to introduce longer PRN signals rather than narrowing down the bandwidth, i.e., moving the working point toward higher N_{sym} direction along the maximum FOM line. On the one hand, high precision is sustainable when surfing from signal attenuation at distal positions, which is demonstrated by the black and purple dots in Fig. 11. On the other hand, longer PRN codes possess better capability against multiplexing interference from other objects. At the end,

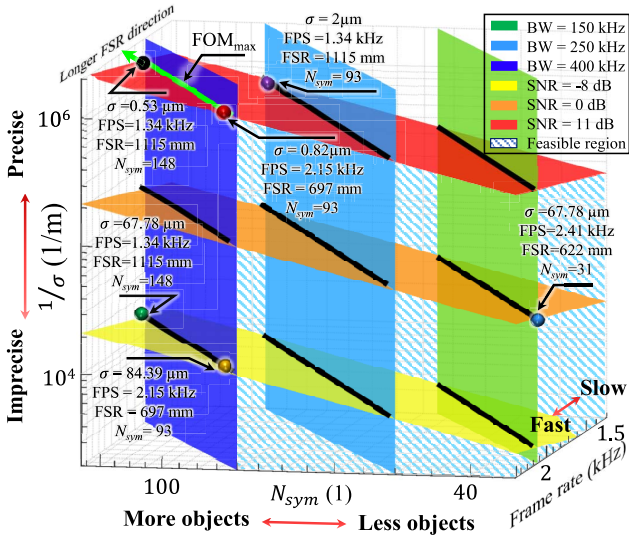


Fig. 11. FOM of correlation-based ranging systems in log scale, where overall ranging performance with different values of SNR and bandwidth is indicated.

in order to realize all desired performance metrics simultaneously, one would need to determine the maximum SNR and bandwidth of the system. In this way, desired precision, multiplexing capacity, and frame rate can be freely achieved by selecting appropriate parameters within the feasible region, which is addressed by the blue and green dots in Fig. 11.

IV. CONCLUSION AND OUTLOOK

In this article, we improved the combination of correlation ToF and carrier shift detection ranging technique by introducing an analog I/Q down-conversion scheme that allows for a zero-IF baseband signal operation and a direct carrier phase shift detection. In this way, the spatial resolution is dominated by the digitization resolution of the ADC in the receiver circuit, and an effective F_s/F_c value of 2 allows to reduce the complexity of the signal processing and the cost of the systemic infrastructure. We analyze and provide relations between technical parameters of the system hardware, ranging signals, and the ranging performance. We verified these performances in a dual-transducer-through-transmission setup in water. We used QAM modulated waveforms of 1023-bit Gold codes with an 8 MHz carrier and 400 kHz bandwidth as ranging signals. The received ranging signal was first down converted and the recovered baseband signal was sampled at an 8 MHz rate using 2×10 -bit ADCs. The combination of carrier phase detection and digital correlation of PRN sequences allowed us to reach submicrometer ranging resolution, an accuracy of $2.31 \mu\text{m}$, and a precision of $0.82 \mu\text{m}$ at 2.15 kHz frame rate within an intermediate distance of 200 mm using simplified electronics. Using a high-density QAM scheme, the multiplexing capacity of six simultaneous signals (objects) was experimentally demonstrated. Such a ranging performance can serve various applications where accurate and precise positions of objects are required to be updated at a high speed with high resolution.

Moreover, an FOM indicating the overall performance upper bound of such ranging systems is defined, and the method to approach the upper bound addressing an optimal set of technical parameters is analyzed. For further improvements, PRN codes with ideal orthogonality should be explored to enhance the multiplexing capacity while keeping the accuracy and precision at a high level [49], especially to overcome the so-called near-far effect occurring when amplitudes of different ranging signals are in huge contrast due to various reasons in real applications. The high-performance ranging technique should eventually be demonstrated in a real application scenario such as tracking a single or multiple small-scale autonomous object(s) using optimal parameters.

ACKNOWLEDGMENT

The authors would like to thank C. Krien as well as K. Leger for lab assistance. The support in the development of the experimental setups from the research technology department of the Leibniz IFW Dresden and the clean room team headed by R. Engelhard (Leibniz IFW Dresden) is greatly appreciated. The authors thank R. Ravishankar for necessary discussions.

V. DATA AVAILABILITY

The authors declare that all data supporting the findings of this study are available within this article.

REFERENCES

- [1] F. Zhou, X. Li, and Z. Wang, "Efficient high cross-user recognition rate ultrasonic hand gesture recognition system," *IEEE Sensors J.*, vol. 20, no. 22, pp. 13501–13510, Nov. 2020, doi: [10.1109/JSEN.2020.3004252](https://doi.org/10.1109/JSEN.2020.3004252).
- [2] Z. Wang *et al.*, "Hand gesture recognition based on active ultrasonic sensing of smartphone: A survey," *IEEE Access*, vol. 7, pp. 111897–111922, 2019, doi: [10.1109/ACCESS.2019.2933987](https://doi.org/10.1109/ACCESS.2019.2933987).
- [3] Y. Sang, L. Shi, and Y. Liu, "Micro hand gesture recognition system using ultrasonic active sensing," *IEEE Access*, vol. 6, pp. 49339–49347, 2018, doi: [10.1109/ACCESS.2018.2868268](https://doi.org/10.1109/ACCESS.2018.2868268).
- [4] R. Carotenuto, M. Merenda, D. Iero, and F. G. D. Corte, "Ranging RFID tags with ultrasound," *IEEE Sensors J.*, vol. 18, no. 7, pp. 2967–2975, Apr. 2018, doi: [10.1109/JSEN.2018.2806564](https://doi.org/10.1109/JSEN.2018.2806564).
- [5] D. Šoštarić and G. Mester, "Drone localization using ultrasonic TDOA and RSS signal: Integration of the inverse method of a particle filter," *FME Trans.*, vol. 48, no. 1, pp. 21–30, 2020, doi: [10.5937/fmet2001021S](https://doi.org/10.5937/fmet2001021S).
- [6] R. Carotenuto, M. Merenda, D. Iero, and F. G. Della Corte, "An indoor ultrasonic system for autonomous 3-D positioning," *IEEE Trans. Instrum. Meas.*, vol. 68, no. 7, pp. 2507–2518, Jul. 2019, doi: [10.1109/TIM.2018.2866358](https://doi.org/10.1109/TIM.2018.2866358).
- [7] F. Tatar, J. R. Mollinger, J. Bastemeijer, and A. Bossche, "Time of flight technique used for measuring position and orientation of laparoscopic surgery tools," in *Proc. IEEE SENSORS*, vol. 3, Oct. 2004, pp. 1480–1483, doi: [10.1109/icsens.2004.1426467](https://doi.org/10.1109/icsens.2004.1426467).
- [8] V. K. Bandari *et al.*, "A flexible microsystem capable of controlled motion and actuation by wireless power transfer," *Nature Electron.*, vol. 3, no. 3, pp. 172–180, Mar. 2020, doi: [10.1038/s41928-020-0384-1](https://doi.org/10.1038/s41928-020-0384-1).
- [9] M. Medina-Sánchez and O. G. Schmidt, "Medical microbots need better imaging and control," *Nature*, vol. 545, no. 7655, pp. 406–408, May 2017, doi: [10.1038/545406a](https://doi.org/10.1038/545406a).
- [10] B. Rivkin *et al.*, "Shape-controlled flexible microelectronics facilitated by integrated sensors and conductive polymer actuators," *Adv. Intell. Syst.*, vol. 3, no. 6, 2021, Art. no. 2000238, doi: [10.1002/aisy.202000238](https://doi.org/10.1002/aisy.202000238).
- [11] M. Fluckiger and B. J. Nelson, "Ultrasound emitter localization in heterogeneous media," in *Proc. 29th Annu. Int. Conf. IEEE Eng. Med. Biol. Soc.*, Aug. 2007, pp. 2867–2870, doi: [10.1109/IEMBS.2007.4352927](https://doi.org/10.1109/IEMBS.2007.4352927).

- [12] J. D. J. Gumprecht, T. C. Lueth, and M. B. Khamesee, "Navigation of a robotic capsule endoscope with a novel ultrasound tracking system," *Microsyst. Technol.*, vol. 19, nos. 9–10, pp. 1415–1423, Sep. 2013, doi: [10.1007/s00542-013-1828-6](https://doi.org/10.1007/s00542-013-1828-6).
- [13] A. J. Fleming, "A review of nanometer resolution position sensors: Operation and performance," *Sens. Actuators A, Phys.*, vol. 190, pp. 106–126, Feb. 2013, doi: [10.1016/j.sna.2012.10.016](https://doi.org/10.1016/j.sna.2012.10.016).
- [14] P. Oleksy and Ł. Januszkiwicz, "Wireless capsule endoscope localization with phase detection algorithm and simplified human body model," *Int. J. Electron. Telecommun.*, vol. 66, no. 1, pp. 45–51, 2020, doi: [10.24425/ijet.2019.130264](https://doi.org/10.24425/ijet.2019.130264).
- [15] F. Ullrich *et al.*, "Mobility experiments with microrobots for minimally invasive intraocular surgery," *Investigative Ophthalmol. Vis. Sci.*, vol. 54, no. 4, pp. 2853–2863, 2013, doi: [10.1167/iovs.13-11825](https://doi.org/10.1167/iovs.13-11825).
- [16] S. Schurle *et al.*, "Three-dimensional, automated magnetic biomaniipulation with subcellular resolution," in *Proc. IEEE Int. Conf. Robot. Automat.*, May 2013, pp. 1452–1457, doi: [10.1109/ICRA.2013.6630762](https://doi.org/10.1109/ICRA.2013.6630762).
- [17] X. Shu, B. Liu, and S. Liao, "Research on laser ranging technology based on chaotic pulse position modulation," *Proc. SPIE*, vol. 11455, Apr. 2020, Art. no. 114558D, doi: [10.1117/12.2565422](https://doi.org/10.1117/12.2565422).
- [18] A. Aziz, M. Medina-Sánchez, J. Claussen, and O. G. Schmidt, "Real-time optoacoustic tracking of single moving micro-objects in deep phantom and *ex vivo* tissues," *Nano Lett.*, vol. 19, no. 9, pp. 6612–6620, 2019, doi: [10.1021/acs.nanolett.9b02869](https://doi.org/10.1021/acs.nanolett.9b02869).
- [19] K. Arshak and F. Adepoju, "Object tracking in the GI tract: A novel microcontroller approach," in *Proc. 9th IEEE Int. Workshop Adv. Motion Control*, Mar. 2006, pp. 494–499, doi: [10.1109/AMC.2006.1631709](https://doi.org/10.1109/AMC.2006.1631709).
- [20] X. Chen, J. Xu, H. Chen, H. Ding, and J. Xie, "High-accuracy ultrasonic rangefinders via pMUTs arrays using multi-frequency continuous waves," *J. Microelectromech. Syst.*, vol. 28, no. 4, pp. 634–642, Aug. 2019, doi: [10.1109/JMEMS.2019.2912869](https://doi.org/10.1109/JMEMS.2019.2912869).
- [21] D. Marioli, C. Narduzzi, C. Offelli, D. Petri, E. Sardini, and A. Taroni, "Digital time-of-flight measurement for ultrasonic sensors," *IEEE Trans. Instrum. Meas.*, vol. 41, no. 1, pp. 93–97, Feb. 1992, doi: [10.1109/19.126639](https://doi.org/10.1109/19.126639).
- [22] F. Sunol, D. A. Ochoa, and J. E. Garcia, "High-precision time-of-flight determination algorithm for ultrasonic flow measurement," *IEEE Trans. Instrum. Meas.*, vol. 68, no. 8, pp. 2724–2732, Aug. 2019, doi: [10.1109/TIM.2018.2869263](https://doi.org/10.1109/TIM.2018.2869263).
- [23] R. Queirós, F. C. Alegria, P. S. Girao, and A. C. Serra, "Cross-correlation and sine-fitting techniques for high-resolution ultrasonic ranging," *IEEE Trans. Instrum. Meas.*, vol. 59, no. 12, pp. 3227–3236, Dec. 2010, doi: [10.1109/TIM.2010.2047305](https://doi.org/10.1109/TIM.2010.2047305).
- [24] S. Assous, C. Hopper, M. Lovell, D. Gunn, P. Jackson, and J. Rees, "Short pulse multi-frequency phase-based time delay estimation," *J. Acoust. Soc. Amer.*, vol. 127, no. 1, pp. 309–315, Jan. 2010, doi: [10.1121/1.3263602](https://doi.org/10.1121/1.3263602).
- [25] M. Parrilla, J. J. Anaya, and C. Fritsch, "Digital signal processing techniques for high accuracy ultrasonic range measurements," *IEEE Trans. Instrum. Meas.*, vol. 40, no. 4, pp. 759–763, Aug. 1991, doi: [10.1109/19.85348](https://doi.org/10.1109/19.85348).
- [26] T. Yamada, "High-accuracy estimations of frequency, amplitude, and phase with a modified DFT for asynchronous sampling," *IEEE Trans. Instrum. Meas.*, vol. 62, no. 6, pp. 1428–1435, Jun. 2013, doi: [10.1109/TIM.2013.2239031](https://doi.org/10.1109/TIM.2013.2239031).
- [27] R. Queirós, R. C. Martins, P. S. Girao, and A. Cruz Serra, "A new method for high resolution ultrasonic ranging in air," *Proc. 18th IMEKO World Congr. Metrol. Sustain. Dev.*, vol. 2, 2006, pp. 1078–1081.
- [28] L. Svilainis and V. Dumbrava, "The time-of-flight estimation accuracy versus digitization parameters," *Ultrasound J.*, vol. 63, no. 1, pp. 12–17, 2008.
- [29] L. Segers, D. Van Bavegem, S. De Winne, A. Braeken, A. Touhafi, and K. Steenhaut, "An ultrasonic multiple-access ranging core based on frequency shift keying towards indoor localization," *Sensors*, vol. 15, no. 8, pp. 18641–18665, Jul. 2015, doi: [10.3390/s150818641](https://doi.org/10.3390/s150818641).
- [30] D. Yi, H. Jin, M. C. Kim, and S. C. Kim, "An ultrasonic object detection applying the ID based on spread spectrum technique for a vehicle," *Sensors*, vol. 20, no. 2, p. 414, 2020, doi: [10.3390/s20020414](https://doi.org/10.3390/s20020414).
- [31] J. Wu, J. Zhu, L. Yang, M. Shen, B. Xue, and Z. Liu, "A highly accurate ultrasonic ranging method based on onset extraction and phase shift detection," *Measurement*, vol. 47, pp. 433–441, Jan. 2014, doi: [10.1016/j.measurement.2013.09.025](https://doi.org/10.1016/j.measurement.2013.09.025).
- [32] R. Queirós, F. C. Alegria, P. Silva Girão, and A. Cruz Serra, "A multi-frequency method for ultrasonic ranging," *Ultrasonics*, vol. 63, pp. 86–93, Dec. 2015, doi: [10.1016/j.ultras.2015.06.018](https://doi.org/10.1016/j.ultras.2015.06.018).
- [33] J. C. Jackson, R. Summan, G. I. Dobie, S. M. Whiteley, S. G. Pierce, and G. Hayward, "Time-of-flight measurement techniques for airborne ultrasonic ranging," *IEEE Trans. Ultrason., Ferroelectr., Freq. Control*, vol. 60, no. 2, pp. 343–355, Feb. 2013, doi: [10.1109/TUFFC.2013.2570](https://doi.org/10.1109/TUFFC.2013.2570).
- [34] L. Segers, A. Braeken, and A. Touhafi, "Optimizations for FPGA-based ultrasound multiple-access spread spectrum ranging," *J. Sensors*, vol. 2020, pp. 1–26, Jun. 2020, doi: [10.1155/2020/4697345](https://doi.org/10.1155/2020/4697345).
- [35] F. E. Gueuning, M. Varlan, C. E. Eugne, and P. Dupuis, "Accurate distance measurement by an autonomous ultrasonic system combining time-of-flight and phase-shift methods," *IEEE Trans. Instrum. Meas.*, vol. 46, no. 6, pp. 1236–1240, Dec. 1997, doi: [10.1109/19.668260](https://doi.org/10.1109/19.668260).
- [36] M. M. Saad, C. J. Bleakley, and S. Dobson, "Robust high-accuracy ultrasonic range measurement system," *IEEE Trans. Instrum. Meas.*, vol. 60, no. 10, pp. 3334–3341, Oct. 2011, doi: [10.1109/TIM.2011.2128950](https://doi.org/10.1109/TIM.2011.2128950).
- [37] J. Grossmann, A. Suslov, G. Yong, L. A. Boatner, and O. Svitelskiy, "Highly sensitive simple homodyne phase detector for ultrasonic pulse-echo measurements," *Rev. Sci. Instrum.*, vol. 87, no. 4, 2016, Art. no. 044901, doi: [10.1063/1.4945361](https://doi.org/10.1063/1.4945361).
- [38] P. Dycka, P. Janu, J. Bajer, and R. Bystricky, "Phase-coded modulation-based time-of-flight measurement improvement for piezoelectric ceramic transducers," *IEEE Trans. Ultrason., Ferroelectr., Freq. Control*, vol. 68, no. 4, pp. 1362–1369, Apr. 2021, doi: [10.1109/TUFFC.2020.3029329](https://doi.org/10.1109/TUFFC.2020.3029329).
- [39] M. H. AlSharif, M. Saad, M. Siala, T. Ballal, H. Boujemaa, and T. Y. Al-Naffouri, "Zadoff-Chu coded ultrasonic signal for accurate range estimation," in *Proc. 25th Eur. Signal Process. Conf. (EUSIPCO)*, Aug. 2017, pp. 1250–1254, doi: [10.23919/EUSIPCO.2017.8081408](https://doi.org/10.23919/EUSIPCO.2017.8081408).
- [40] Y. Wang, T. Suginochi, M. Hashimoto, and H. Hachiya, "Automatic interference elimination algorithm for ultrasonic multiple access method," *Jpn. J. Appl. Phys.*, vol. 47, no. 5, pp. 4319–4324, May 2008, doi: [10.1143/JJAP.47.4319](https://doi.org/10.1143/JJAP.47.4319).
- [41] M. Golay, "Complementary series," *IRE Trans. Inf. Theory*, vol. 7, no. 2, pp. 82–87, Apr. 1961, doi: [10.1109/TIT.1961.1057620](https://doi.org/10.1109/TIT.1961.1057620).
- [42] P. R. N. Code. (2022). *October 2020 Edition L1 C / A PRN CODE ASSIGNMENTS Changes Shown in Bold Please Refer to IS-GPS-200 for Published Values October 2020 Edition L1 C / A PRN CODE ASSIGNMENTS Please Refer to IS-GPS-200 for Published Values*. [Online]. Available: <https://www.gps.gov/technical/icwg/>
- [43] W. M. D. Wright, O. M. Doyle, and C. T. Foley, "P2I-9 multi-channel data transfer using air-coupled capacitive ultrasonic transducers," in *Proc. IEEE Ultrason. Symp.*, vol. 1, Oct. 2006, pp. 1805–1808, doi: [10.1109/ULTSYM.2006.454](https://doi.org/10.1109/ULTSYM.2006.454).
- [44] C. Li, D. A. Hutchins, and R. J. Green, "Short-range ultrasonic digital communications in air," *IEEE Trans. Ultrason., Ferroelectr., Freq. Control*, vol. 55, no. 4, pp. 908–918, Apr. 2008, doi: [10.1109/TUFFC.2008.726](https://doi.org/10.1109/TUFFC.2008.726).
- [45] C. Li, D. A. Hutchins, and R. J. Green, "Short-range ultrasonic communications in air using quadrature modulation," *IEEE Trans. Ultrason., Ferroelectr., Freq. Control*, vol. 56, no. 10, pp. 2060–2072, Oct. 2009, doi: [10.1109/TUFFC.2009.1289](https://doi.org/10.1109/TUFFC.2009.1289).
- [46] C. Li, D. Hutchins, and R. Green, "Short-range ultrasonic communications in air," *Commun. Transp. Syst.*, vol. 56, no. 10, pp. 358–396, 2013, doi: [10.4018/978-1-4666-2976-9.ch014](https://doi.org/10.4018/978-1-4666-2976-9.ch014).
- [47] T. L. Szabo, *Diagnostic Ultrasound Imaging: Inside Out*, 2nd ed. Amsterdam, The Netherlands: Elsevier, 2014.
- [48] C. Wang, Y. Yang, and R. Ying, "On the performance of DS spread-spectrum systems in AWGN channel," in *Proc. Int. Conf. Commun. Mobile Comput. (WRI)*, Jan. 2009, pp. 311–315, doi: [10.1109/CMC.2009.258](https://doi.org/10.1109/CMC.2009.258).
- [49] H.-H. Chen, *The Next Generation CDMA Technologies*, 1st ed. West Sussex, U.K.: Wiley, 2007.
- [50] M. M. Ghanbari *et al.*, "A sub-mm³ ultrasonic free-floating implant for multi-mote neural recording," *IEEE J. Solid-State Circuits*, vol. 54, no. 11, pp. 3017–3030, Nov. 2019, doi: [10.1109/JSSC.2019.2936303](https://doi.org/10.1109/JSSC.2019.2936303).
- [51] L. Jia *et al.*, "A high-resolution ultrasonic ranging system using laser sensing and a cross-correlation method," *Appl. Sci.*, vol. 9, no. 7, p. 1483, Apr. 2019, doi: [10.3390/app9071483](https://doi.org/10.3390/app9071483).

- [52] O. Wind, "Adaptive channel estimation and data detection for underwater acoustic MIMO-OFDM systems," *IEEE J. Ocean. Eng.*, vol. 36, no. 4, pp. 837–846, Jul. 2011, doi: [10.1109/JOE.2010.2052326](https://doi.org/10.1109/JOE.2010.2052326).



Zehua Dou received the M.Sc. degree in micro and nanosystems from TU Chemnitz, Chemnitz, Germany, in 2019. Currently, he is pursuing the Ph.D. degree in electronics with the Leibniz Institute for Solid State and Materials Research Dresden (Leibniz IFW Dresden), Dresden, Germany.

His research focuses on signal processing techniques of various medical imaging instrumentations addressing ultrasound and magnetic fields, materials, and physics aiming at actuating and sensing medical autonomous systems including piezoelectric, magnetostrictive materials, as well as bubble dynamics and cavitation.

as well as bubble dynamics and cavitation.



Dmitriy Karnaushenko received the Dr.-Ing. degree from Chemnitz University of Technology, Chemnitz, Germany, in 2017, for his work on self-assembled helical antennas.

He started as a Post-Doctorate Researcher at the Leibniz Institute for Solid State and Materials Research Dresden (Leibniz IFW Dresden), Dresden, Germany, in 2017. His research focuses on self-assembling electronic devices, FEM simulations for mechanical, and electrical and microfluidic devices.



Oliver G. Schmidt received the Dr.rer.nat. degree from TU Berlin, Berlin, Germany, in 1999.

From 2007 to 2021, he was the Director of the Institute for Integrative Nanosciences, Leibniz IFW Dresden, Dresden, Germany. He holds a Full Professorship for Materials Systems for Nanoelectronics at Chemnitz University of Technology, Chemnitz, Germany. He is an Adjunct Professor for Nanophysics at Dresden University of Technology, Dresden, and holds an Honorary Professorship at Fudan University, Shanghai, China. His interdisciplinary activities

bridge across several research fields, ranging from flexible electronics and microbotics to energy storage and nanophotonics.



Daniil Karnaushenko received the Dr.-Ing. degree from Chemnitz University of Technology, Chemnitz, Germany, in 2016, for his work on shapeable electronics, after studying at Novosibirsk State Technical University, Novosibirsk, Russia.

He started as a Post-Doctorate Researcher at the Leibniz Institute for Solid State and Materials Research Dresden (Leibniz IFW Dresden), Dresden, Germany, in 2016. His research focuses on novel microfabrication processes, including self-assembly techniques and microelectronics.